# Preparation and Mechanical Properties of Mullites and Mullite-Zirconia Composites

Yoshitaka KUBOTA
Hiroyoshi TAKAGI*

High-purity stoichiometric mullite and mullite-zirconia composite powders were prepared by calcination of the products precipitated from two different systems of an aqueous solution of $Al(NO_3)_3$/colloidal $SiO_2$ and $Al(NO_3)_3/ZrOCl_2$/colloidal $SiO_2$. The precipitated products transformed into mullite via an exothermic reaction at 1250°C. Tetragonal $ZrO_2$ particles were formed above 800°C in the composite powders. In the range of 70 to 78 wt% $Al_2O_3$, the pure mullite containing 70 and 72 wt% $Al_2O_3$ showed the highest fracture strength above 1000°C because of a glassy phase present along the grain boundaries and the acicular grain shape. On the other hand, fracture strength of mullite-$ZrO_2$ composites increased with increasing $ZrO_2$ volume fraction. Dispersion of $ZrO_2$ particles enhanced the strength of the matrix in a temperature range from room temperature to 900°C. The toughening mechanism seems to be a combination of transformation toughening and other mechanisms such as microcracking and/or crack deflection.

## 1. Introduction

Mullite is one of the basic constituents of traditional refractories. It is attractive because of its high temperature mechanical stability, creep resistance, chemical resistance, low thermal expansion and dielectric constant. However, since mullite is difficult to be consolidated into fully dense, high-purity stoichiometric bodies. To overcome these difficulties, some investigators have attempted to prepare high-purity and active mullite powders, using co-precipitation[1], organo-metallic[2] and freeze-drying[3] procedures.

In the present study, fine, high-purity powders were prepared by calcination of the products precipitated from mixed aqueous solutions of aluminium nitrate 9-hydrate and colloidal silica. After an appropriate consolidation process, the mechanical properties of the ceramics, such as fracture strength, fracture toughness and slow crack growth behavior, were studied at room temperature to 1400°C.

Mullite-zirconia composites was also prepared using a similar method. This is attempted in view of the previous reports in the literature[4,5,6] that dispersed $ZrO_2$ particles significantly improve the fracture property of the mullite composites.

## 2. Experimental Procedures

### 2—1. Powder preparation

A co-precipitation method using an aqueous solution of (a) $Al(NO_3)_3$ and colloidal $SiO_2$ and (b) $Al(NO_3)_3$, $ZrOCl_2$ and colloidal $SiO_2$ was employed. A typical procedure was conducted as follows:

*Government Industrial Research Institute, Nagoya, JAPAN

an aqueous solution of $NH_4OH$ (14 wt%$NH_3$) was quickly added to an aqueous solution of $Al(NO_3)_3$ containing colloidal $SiO_2$ to form a gel under the condition of continuous stirring, with the pH of the solution adjusted to fall into between 6.5 and 7.5 so that it gives the minimum solubility of $Al(OH)_3$. The mixed hydroxide prepared was then filtered on a Büchner funnel, and the precipitate was washed using distilled water. The precipitate was dried on a shallow tray at 80°C overnight, followed by calcining in an $Al_2O_3$ crucible at 1300°C for 1 h. The calcined material was wet ball-milled for 72 h in an alumina jar using alumina balls and ethanol. After ball-milling the slurry was dried to produce fine mullite powders.

Powder characterization by X-ray diffraction and DTA was made, and the particle morphology of the powders was examined by TEM.

2—2. Consolidation and Testing

About 10 g of prepared powders were cold die-pressed into rectangular blocks, followed by cold isostatic pressing at a total pressure of 250MPa. The compacts were consolidated by pressureless sintering in an electric furnace in air.

Sintered bodies were machined into test bars (3.5 cm by 0.4 cm by 0.3 cm). All faces were ground in the lengthwise direction using 400 grit diamond wheels and the edges were chamfered to prevent notch effects. The surface to be submitted to tension in bending for the measurements of fracture toughness was carefully ground and wet polished to 3 $\mu$m diamond finish.

The fracture strength of the materials was measured by a three-point bending method in a testing machine operated at a constant cross-head speed of 0.5 mm/min, where the span was fixed as 3.0 cm. The controlled surface flaw method[7] using Knoop Diamond microhardness indentation was also used to measure the fracture toughness. A 9.8 N indentation load was used to produce a nearly semicircular microcrack having a radius of $\cong$130 $\mu$m. The testing for fracture strength was done at room temperature to 1400°C in air. Prior to loading, specimens were held at the test temperature for about 15 min in order to achieve thermal equilibrium. Fracture surfaces were examined by SEM. Tetragonal $ZrO_2$ fraction was measured on an as-sintered surface using integrated X-ray diffraction intensities[8]. The micro-indentation method[9] was also used to measure the fracture toughness.

## 3. Results and Discussion

3—1. Powders preparation

The DTA heating curve obtained for the co-precipitated powder with $Al_2O_3/SiO_2$=72/28 (in weight) is shown in Fig. 1. A broad endotherm at 200°C due to the loss of water and two exothermic peaks at 260°C and 1250°C can be seen. The first exotherm at 260°C is attributed to decomposition of nitrate ($NH_4NO_3$). To investigate the origin of the second exotherm, X-ray powder diffraction patterns were obtained for the precipitates submitted to the DTA near 1250°C. The results are shown in

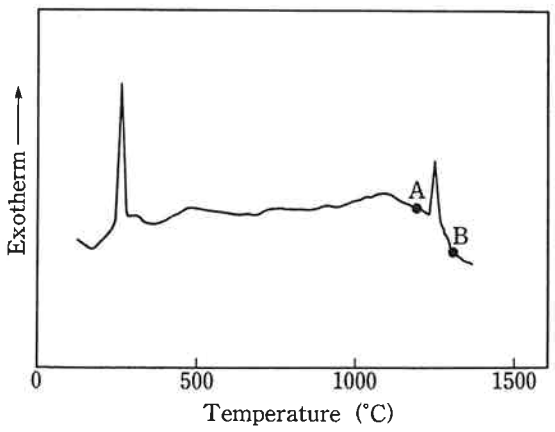


Fig. 1. The DTA heating curve obtained for the co-precipitated powder with $Al_2O_3/SiO_2$ =72/28 (in weight).

Fig. 2. The X-ray chart obtained at point A in the DTA curve shows that the precipitate is a mixture of a $\gamma$-$Al_2O_3$-like phase and amorphous $SiO_2$ (or fine crystalline of cristobalite[10]), and the X-ray chart at point B shows the presence of mullite phase with no evidence of crystalline $Al_2O_3$ and $SiO_2$. These X-ray data suggests that the second exotherm at 1250°C is due to the formation of mullite. Previously, Hoffman et al.[10] reported that gels prepared by gelling colloidal $SiO_2$ and $Al(NO_3)_3$ showed no trace of the exotherm of mullite formation. Instead, there was an apparently continuous reaction over a range of several hundred degrees. The different behaviour between these two studies are likely due to the difference in the degree of mixing between $Al(OH)_3$ and $SiO_2$ in the gel. Fig. 3. is a TEM photograph of the precipitate heated at 1000°C for 1 h. It may be recognized that $Al(OH)_3$ and $SiO_2$ particles in the co-precipitated powder are well mixed and their average grain sizes are in the range of 10 to 40 nm. Metakaolinite[11] and a gel derived from metal alkoxides[1], in which $Al_2O_3$ and $SiO_2$ were mixed on the unit-cell scale, have been reported to indicate two exotherms at 960°C and 1250°C in the DTA curve. The exotherm at 960°C was attributed to both mullite formation and Al-Si spinel formation, while the exotherm at 1250°C was attributed to the transformation of the spinel to mullite. On the other hand, Kanzaki et al.[12] found that amorphous mullite transformed to mullite with an exotherm at 960°C. They reported that the amorphous mullite was prepared by spray pyrolysis of a mixed solution of $Al(NO_3)_3$ and ethylsilicate, where Al and Si ions were considered to be mixed on the atomic scale. These results all suggest that the degree of mixing of Al and Si ions in the co-precipitated powders significantly influence the mullitization temperature.

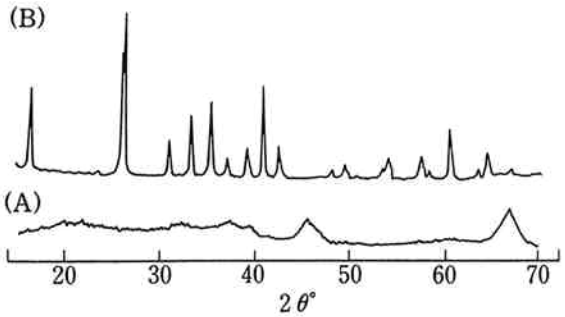


Fig. 2. X-ray powder diffraction patterns obtained for the precipitates which were submitted to the DTA experiments.

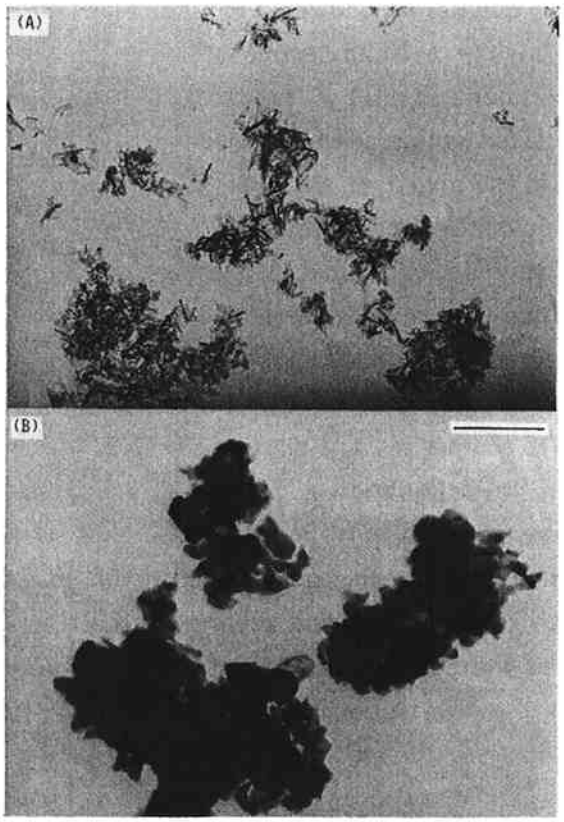


Fig. 3. TEM photogsaphs of the precipitates heated
(A) at 1000°C for 1 h,
(B) at 1300°C for 1 h, (bar=0.2 $\mu$m).

X-ray diffraction patterns for the precipitates of mullite-zirconia composites, which were calcined

at various temperatures, are shown in Fig. 4. These data show that $Zr(OH)_4$ was amorphous below 800°C and tetragonal $ZrO_2$ formed above 800°C in the composite. The formation of mullite phase again occurred by an exothermic reaction at 1250°C.

A TEM photograph of the mullite–$ZrO_2$ composite powders calcined at 1300°C for 1 h is shown in Fig. 5. It was found that dark particles were t–$ZrO_2$ particles surrounded by the mullite agglomerates, which was confirmed by electron diffraction pattern of the particles shown in Fig. 5(B).

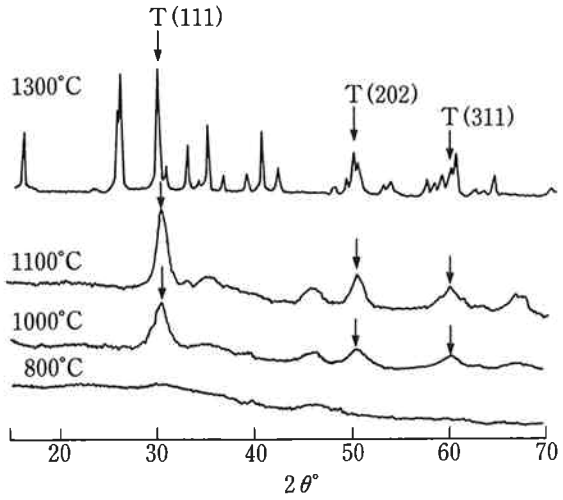


Fig. 4. X-ray diffraction patterns for the precipitates of mullite–zirconia composites, which were calcined at various temperature.

3—2. Microstructures of sintered bodies.

SEM microphotographs of etched surfaces of pure mullite are shown in Fig. 6. In specimen A, mainly acicular grains are seen, while in specimens B and C microstructures are of equiaxed grains, with $\alpha$–$Al_2O_3$ particles dispersed in the matrix of specimen C. The apparently unique microstructure observed in specimen A may be explained in terms of the large amount of the liquid phase formed during sintering[13].

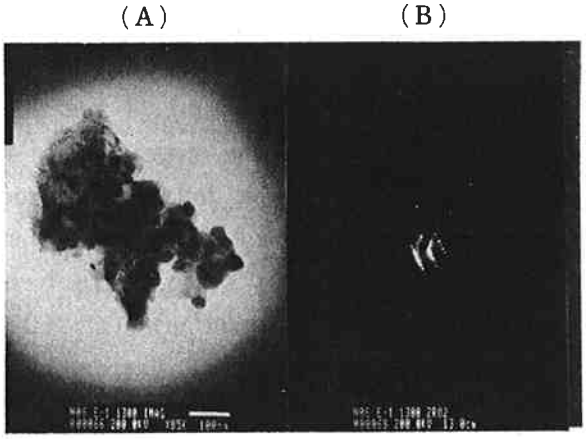


Fig. 5. (A): A TEM photograph of the mullite–$ZrO_2$ composite powder calcined at 1300°C for 1 h, (B): the electron diffraction pattern of the dark particle.

SEM and TEM photographs of the mullite–$ZrO_2$ composites are shown in Fig. 7. Dense mullite–$ZrO_2$ bodies, having $ZrO_2$ particles dispersed uniformly in the matrices, were obtained. As for the microstructure of mullite–$ZrO_2$ composites, it was reported that $ZrO_2$ particles were either inter- or intragranular, depending on the fabrication methods[14]. $ZrO_2$ particles were mainly intragranular in the mullite–$ZrO_2$ composites fabricated by reaction sintering of $Al_2O_3$ and $ZrSiO_4$ powder mixtures, while they were intergranular when the composites were formed using the mechanical mixture of fused mullite and $ZrO_2$ powders. In the present studies using the co-precipitate as the starting powder, most of $ZrO_2$ particles were intergranular, but about 3% of $ZrO_2$ particles were intragranular as shown in Fig. 7(C), (D), (E).

On the other hand, an interesting phenomenon could be seen with regard to the grain morphology of the mullite matrices. In Fig. 7(C), (D), (E), the microstructure of the mullite matrices were same as that of pure mullite.

3—3. Mechanical properties

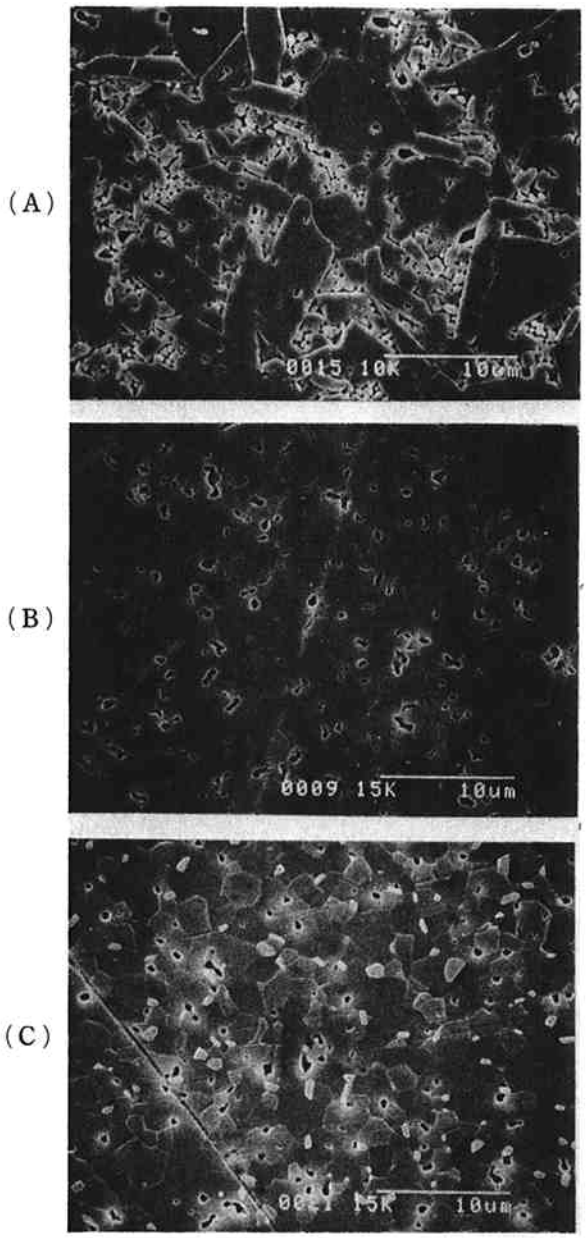


Fig. 6. SEM microphotographs of etched surface of mullites and mulite-zirconia composites, (A), (B), (C): sintered at 1650°C, 3 h.

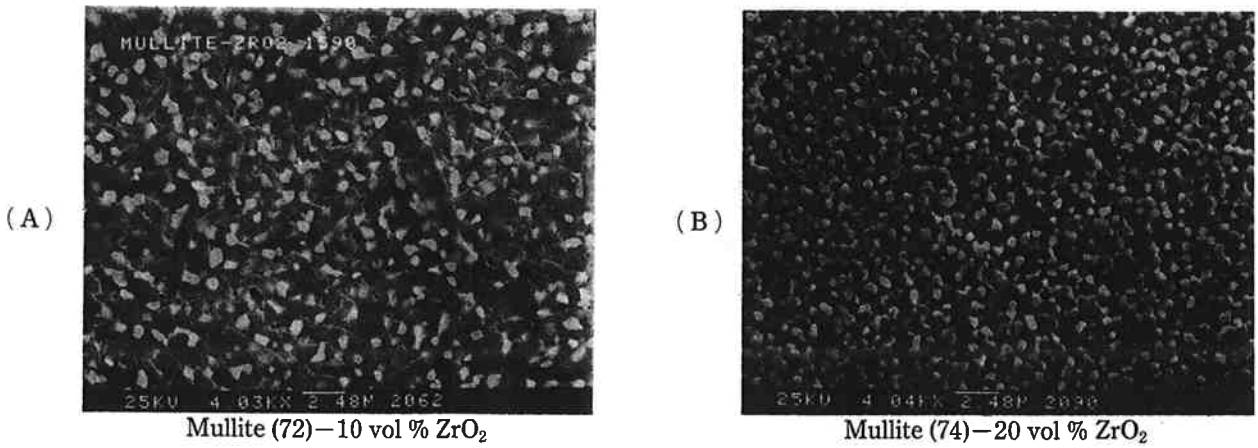


Mullite (72)−10 vol % $ZrO_2$ Mullite (74)−20 vol % $ZrO_2$

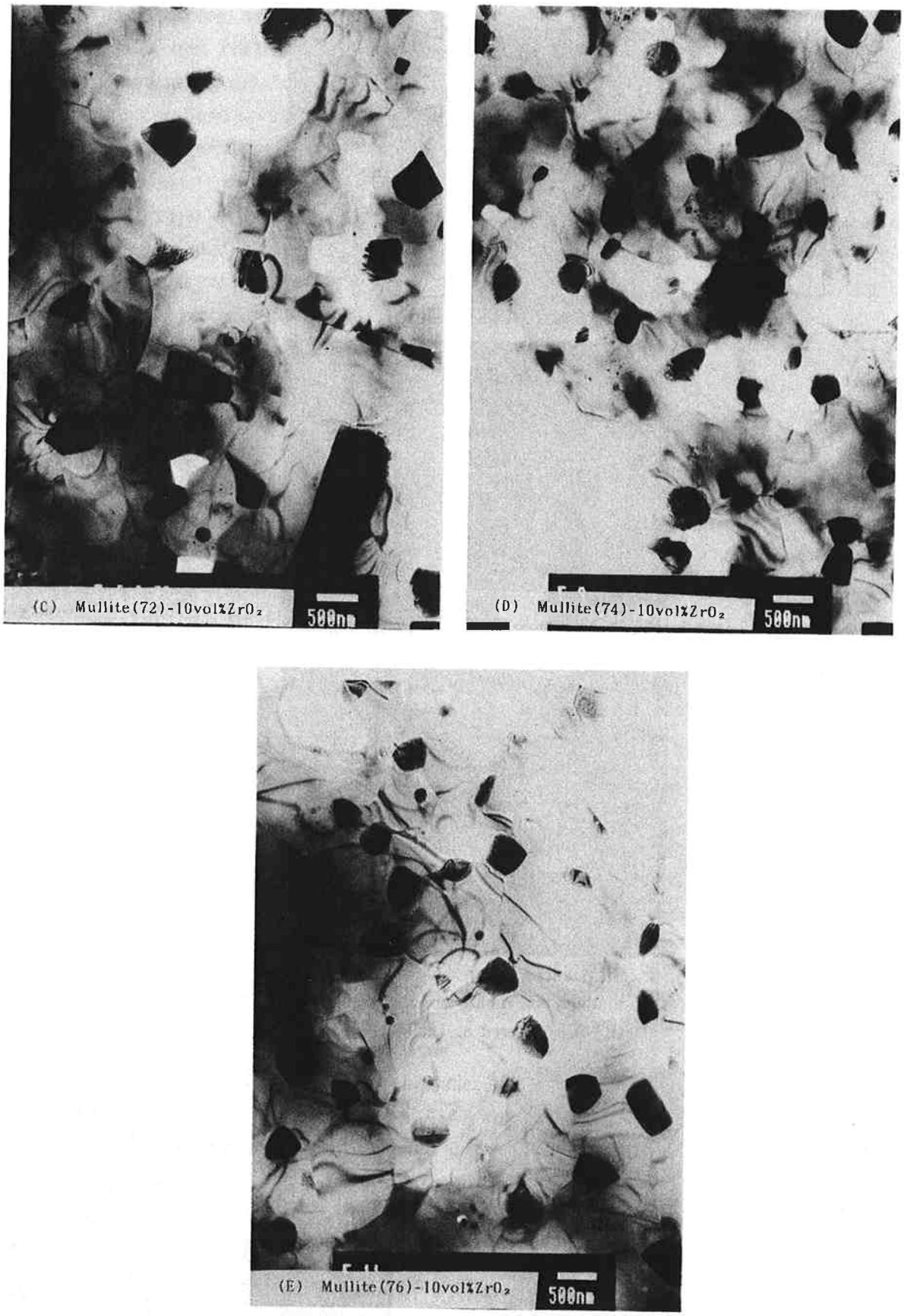


Fig. 7. SEM and TEM photographs of the mullite–$ZrO_2$ composites, (A) (C) (D) and (E) sintered at 1620°C for 3 h, (B) at 1590°C for 3 h.

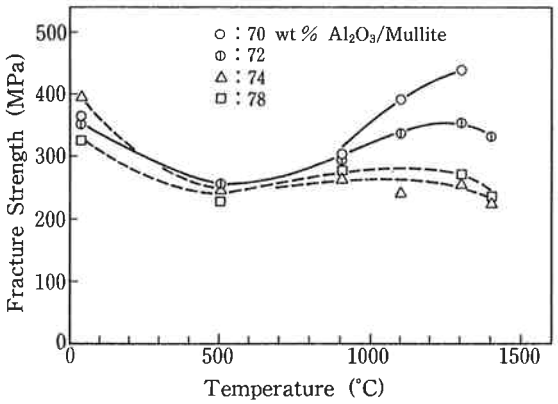


Fig. 8. The temperature dependence of fracture strength obtained for the specimens with $Al_2O_3$ contents in the range of 70 to 78 wt%, all specimens were sintered at 1650°C, 3 h.

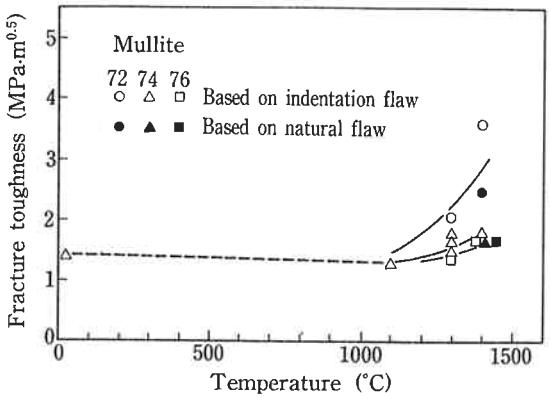


Fig. 9. Fracture toughness for specimens with 72, 74 and 76 wt% $Al_2O_3$ sintered at 1700°C plotted as a function of temperature.

3—3—1. Mullite

The results of bending strength between room temperature and 1400°C for four compositions of $Al_2O_3/SiO_2$ are shown in Fig. 8. From these results, it is found that the fracture strength is essentially independent of composition from room temperature to 900°C, with the minima in all the strength curves around 500°C. This figure also shows that in the temperature range of 900°C to 1300°C mullites with 70 and 72 wt% $Al_2O_3$ exhibite a significant increase in their fracture strength, while mullites with 74 and 78 wt% $Al_2O_3$ have little or no change. Fig. 9. shows $K_{1c}$ for specimens with 72, 74 and 76 wt% $Al_2O_3$ at various temperatures. In this figure, the $K_{1c}$ values obtained using the fracture-initiating flaw size, measured by SEM fractography are also shown as full symbols. Typical fracture topographies of the specimens precracked and tested at 1300°C and 1400°C are shown in Fig. 10. Although the fracture surface of a specimen tested at 1100°C did not reveal the presence of slow crack growth (SCG), in the specimen tested at 1300°C and 1400°C SCG this was observed. Completely intergranular fracture can be seen in the SCG region in the SEM microphotographs of Fig. 10. Mullites with 70 and 72 wt% $Al_2O_3$ were found to increases in both $\sigma_f$ and $K_{1c}$ above 1300°C, where SCG was observed. These increases in $\sigma_f$ and $K_{1c}$ were explained by the dominance of energy dissipation through plastic relaxation in the plastic zone over grain boundary sliding due to the presence of a glassy phase[15]. The appearance of SCG around 1300°C and above suggests the presence of an amorphous phase along the grain boundaries. It seems that the amount of the glassy phase at the grain boundary of mullite increases with decreasing $Al_2O_3$ content. The glassy phase seems to contribute to the fracture strength more in mullite with 70 and 72 wt% $Al_2O_3$ than those with 74 and 78 wt% $Al_2O_3$. The other contributing cause for the higher strength in mullite with 70 wt% $Al_2O_3$ is the non-equiaxed and grain structure which suppresses gross deformation and deflects crack propagation.

3—3—2. Mullite-zirconia composites

Fracture strength and toughness at room temperature as a function of $ZrO_2$ volume fraction of two different $Al_2O_3$ to $SiO_2$ ratio in mullite are shown in Fig. 11. The fracture strength and toughness

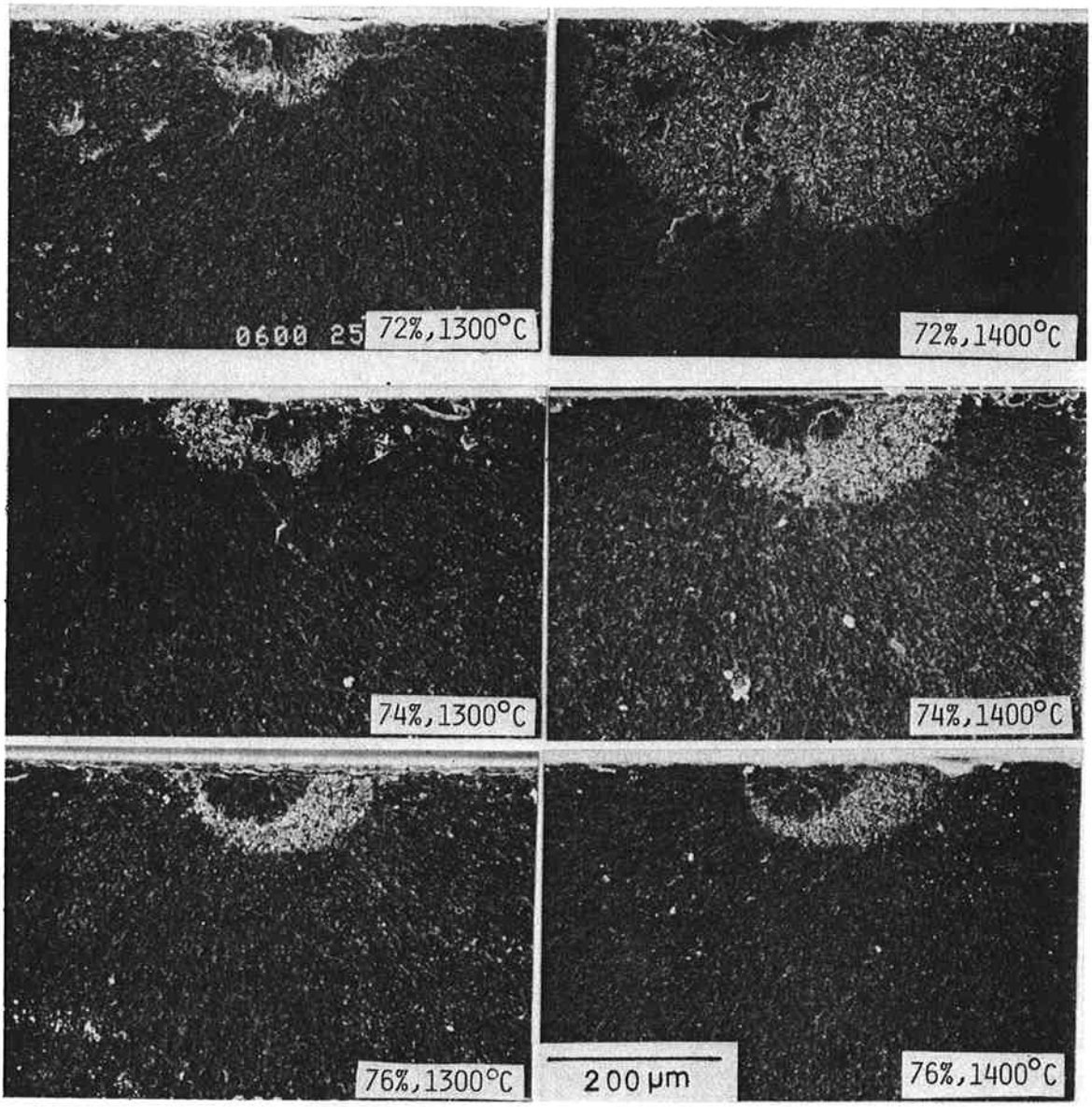


Fig. 10. Typical fracture topographies of the specimens precracked and tested at 1300°C and 1400°C.

increased with increasing total $ZrO_2$ volume fraction. As seen in Fig. 12, when the total $ZrO_2$ volume fraction in the mullite–$ZrO_2$ composites increased, the grain size of $ZrO_2$ increased, and the tetragonal fraction of $ZrO_2$ sharply decreased. As compared with the results of the composite fabricated by milling of fused mullite and $ZrO_2$ powder[16], the increase in $ZrO_2$ particle size was small, while the t–$ZrO_2$ fraction decreased significantly. The stability of t–$ZrO_2$ particles in ceramic matrices depends on the particle characteristics such as its size, shape, and distribution; furthermore, it seems to be influenced by the constrictive force acting on the $ZrO_2$ particles in the $ZrO_2$ toughened ceramics. Increasing the $ZrO_2$ fraction reduces the constrictive force exerted on $ZrO_2$. Furthermore, as shown in Fig. 7, most of the $ZrO_2$ particles were intergranular in the present mullite–$ZrO_2$ composites. Intergranular particles are less resistant to transformation, because they are less stable than intragranular particles[17]. In mullite–10 vol% $ZrO_2$ composite the fracture toughness increased with increasing t–$ZrO_2$ fraction as shown in Fig. 13. This fact indicats that

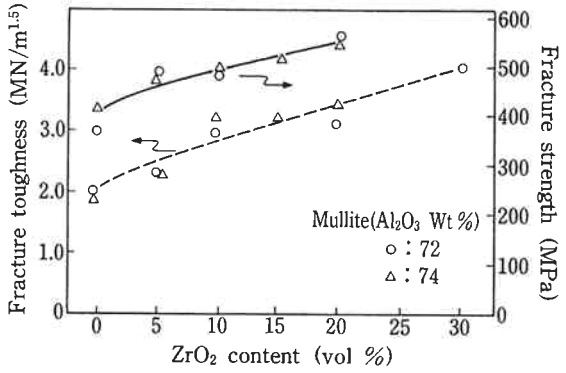


Fig. 11. Fracture strength and toughness at room temperature as a function of $ZrO_2$ volume fraction for two compositions of $Al_2O_3/SiO_2$, specimens (except the mullite-10 vol% $ZrO_2$ sintered at 1610°C for 3 h) were sintered at 1590°C for 3 h.

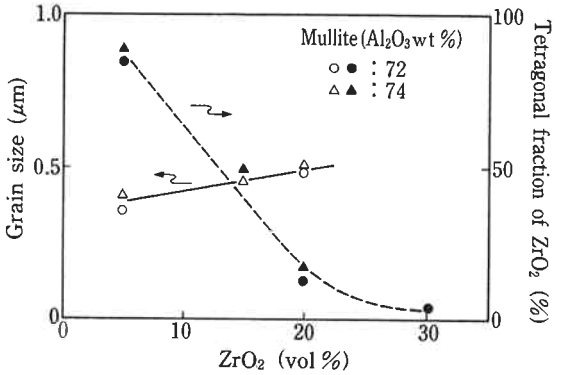


Fig. 12. $ZrO_2$ particle size and tetragonal fraction of $ZrO_2$ as a function of total $ZrO_2$ volume fraction, sintering conditions were the same as in Figure-3.

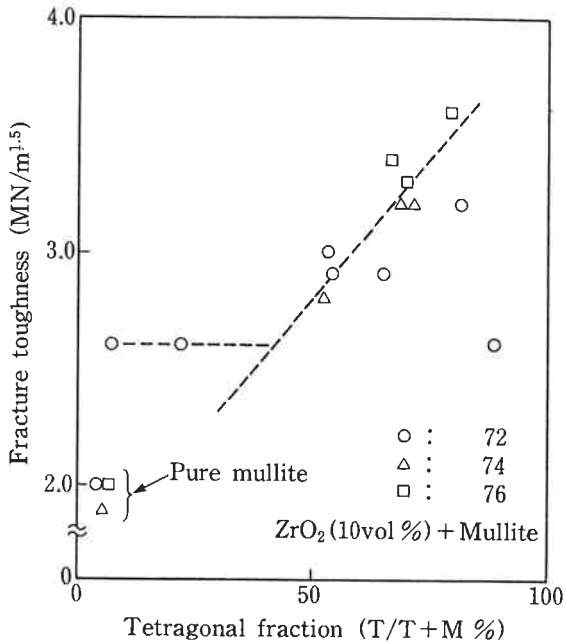


Fig. 13. The fracture toughness as a function of tetragonal $ZrO_2$ fraction in the mullite-10 vol% $ZrO_2$ composites, the fraction of t-$ZrO_2$ were controlled by sintering at different temperatures.

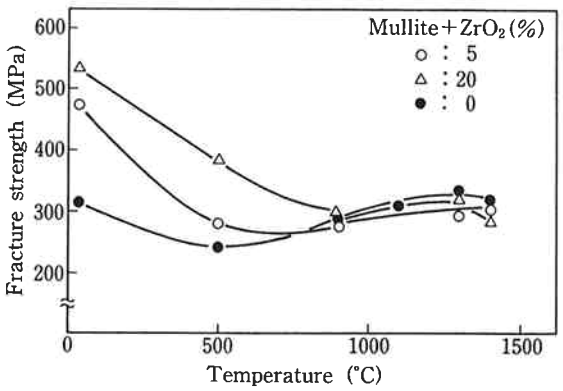


Fig. 14. The temperature dependence of the fracture strength of the composites mullite (72)+$ZrO_2$(5 and 20 vol%) sintered at 1590°C for 3 h.

the transformation toughening is one of the toughening mechanisms as reported by Wallace [14]. On the other hand, the extrapolated fracture toughness value at $ZrO_2=0$ does not coincide with the measured value of pure mullite, which indicats that other toughening mechanisms such as micro-cracking[18] and crack deflection[19] are activated in the present composites.

The temperature dependence of the fracture strength of the composites mullite(72)+$ZrO_2$(5 and 20 vol%) and mullite(74)+$ZrO_2$(5, 15 and 20 vol%) are shown in Fig. 14 and15. The fracture strength of all specimens was higher than that of pure mullite. The fracture strength decreased monotonically with increasing temperatures up to 900°C, and approached the same value of mullite (72 and 74) with no $ZrO_2$ additions at 900°C. In the temperature range of 900°C to 1300°C, the

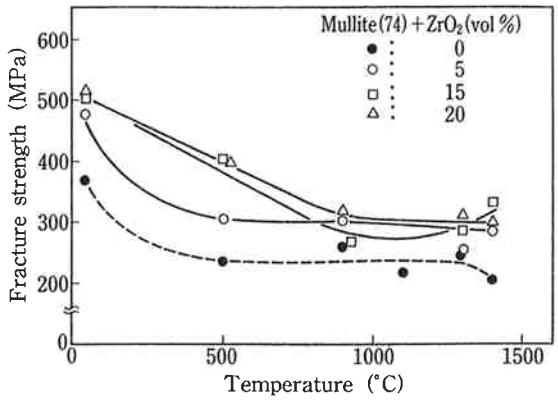


Fig. 15. The temperature dependence of the fracture strength of the composites mullite(74)+$ZrO_2$(5, 15 and 20 vol%) sintered at 1590°C for 3 h.

temperature dependence of the strength of the composites seems to be generally similar to that of pure mullite without effects of t-$ZrO_2$ on fracture strength by toughening and of little contribution of both micro-cracking and crack deflection.

## 4. Conclusion

1) The products precipitated from aqueous solution of $Al(NO_3)_3$ mixed with colloidal $SiO_2$ transform to mullite with an exotherm reaction at 1250°C.

2) In the range of 70 to 78 wt% $Al_2O_3$, the composition 70 wt% $Al_2O_3$ shows the highest fracture strength above 1000°C because of a glassy phase present along the grain boundaries and the acicular grain shape.

3) Dense mullite-$ZrO_2$ composites, having $ZrO_2$ particles dispersed uniformly in the matrices, were obtained form a co-precipitation method. Most of $ZrO_2$ particles were intergranular. Furthermore, the microstructural features of the mullite matrices depend on the $Al_2O_3/SiO_2$ ratios of the mullite.

4) Fracture strength of mullite-$ZrO_2$ composites increased with increasing total $ZrO_2$ volume fraction in a temperature range from room temperature to 900°C. The toughening mechanism seems to be a combination of transformation toughening and other mechanisms such as microcracking and/or crack deflection.

## References

1) H. Yamad and S. Kimura; *J. Ceram. Assoc. Japan,* **70**, 65, 1962.
2) K. S. Mazdiyasni and L. M. Brown; *J. Am. Ceram. Soc.,* **55**, 548, 1972.
3) T. A. Wheat, E. M. H. Sallam and A. C. D. Chaklader; *Ceramurgia Int.,* 2, 42, 1979.
4) N. Claussen and J. Jahn; *J. Am. Ceram. Soc.,* **63**, 228, 1980.
5) G. Orange et al.; *J. Mater. Sci.,* **20**, 2533, 1985.
6) J. S. Moya and M. I. Osendi; *J. Mater. Sci.,* **19**, 2909, 1984.
7) J. J. Petrovic and M. G. Mendiratta; "Fracture Mechanics Applied to Brittle Materials, ASTM. STP 678", Edited by S. W. Freiman, ASTM, pp. 83-102.
8) R. C. Garvie and P. S. Nicholson; *J. Am. Ceram. Soc.,* **55**, 303, 1972.
9) K. Nihara, R. Morena and D. P. Hasselman; *J. Mater. Sci.,* **1**, 13, 1982.
10) D. W. Hoffman, R. Roy and S. Komarneni; *J. Am. Ceram. Soc.,* **67**, 468, 1984.
11) A. K. Chakraborty and D. K. Ghosh; *J. Am. Ceram. Soc.,* **61**, 170, 1978.
12) S. Kanzaki, H. Tabata and T. Kumazawa; *J. Am. Ceram. Soc.,* **68**, c-6, 1985.
13) S. Prochazka and F. J. Klug; *J. Am. Ceram. Soc.,* **66**, 874, 1983.
14) J. S. Wallace, N. Claussen and S. Prochazka; *Proc. of International Synposium on Ceramic components for Engine,* 1983 Japan.
15) TAI-IL MAH and K. S. Mazdiyasni; *J. Am. Ceram. Soc.,* **66**, 700, 1983.